Title

Novel Double-Stage High-Concentrated Solar Hybrid Photovoltaic/Thermal (PV/T) Collector with Nonimaging Optics and GaAs Solar Cells Reflector

Permalink

https://escholarship.org/uc/item/78s917x8

Journal

Applied Energy Journal, 182(15)

Authors
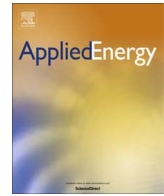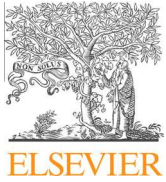
Abdelhamid, Mahmoud
Widyolar, Bennett
Jiang, Lun

Publication Date

2016-07-01

Data Availability

Associated data will be made available after this publication is published.

Peer reviewed

Novel double-stage high-concentrated solar hybrid photovoltaic/thermal (PV/T) collector with nonimaging optics and GaAs solar cells reflector

Mahmoud Abdelhamid [a,*], Bennett K. Widyolar [a], Lun Jiang [a], Roland Winston [a], Eli Yablonovitch [b], Gregg Scranton [b], David Cygan [c], Hamid Abbasi [c], Aleksandr Kozlov [c]

[a] University of California-Merced, 5200 Lake Rd, Merced, CA 95343, USA
[b] University of California-Berkeley, Berkeley, CA USA
[c] Gas Technology Institute, Des Plaines, IL, USA

HIGHLIGHTS

- A novel hybrid concentrating photovoltaic thermal (PV/T) collector is developed.
- Thermal component achieves 60× concentration using nonimaging optics.
- GaAs solar cells used as spectrally selective mirrors for low energy photons.
- Thermal efficiencies of 37% at 365 °C and electrical efficiencies of 8% achieved.
- Combined electric efficiency reaches 25% of DNI for system cost of $283.10/m².

GRAPHICAL ABSTRACT
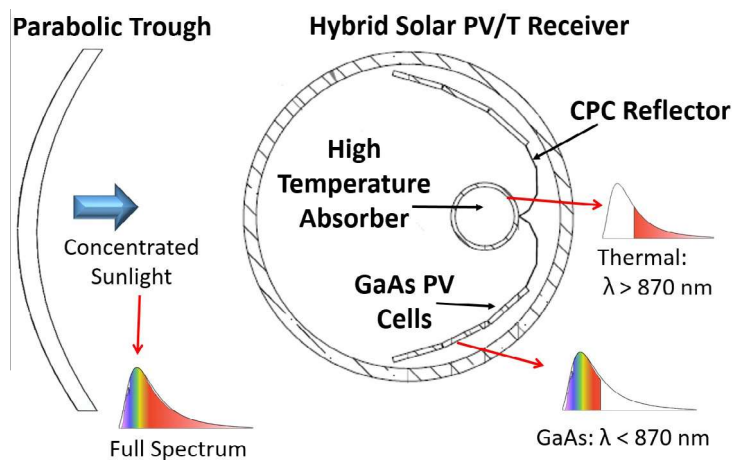
ABSTRACT

A novel double stage high-concentration hybrid solar photovoltaic thermal (PV/T) collector using non-imaging optics and world record thin film single-junction gallium arsenide (GaAs) solar cells has been developed. We present a detailed design and simulation of the system, experimental setup, prototype, system performance, and economic analysis. The system uses a parabolic trough (primary concentrator) to focus sunlight towards a secondary nonimaging compound parabolic concentrator (CPC) to simultaneously generate electricity from single junction GaAs solar cells, as well as high temperature dispatchable heat. This study is novel in that (a) the solar cells inside the vacuum tube act as spectrally selective mirrors for lower energy photons to maximize the system exergy, and (b) secondary concentrator allows the thermal component to reach a concentration ratio ~60×, which is significantly higher than conventional PV/T concentration ratios. The maximum outlet temperature reached was 365 °C, and on average the thermal efficiency of the experiment was around 37%. The maximum electrical efficiency was around 8%. The total system electricity generation is around 25% of incoming DNI, by assuming the high temperature stream is used to power a steam turbine. The installed system cost per unit of parabolic trough aperture area is $283.10 per m².

© 2016 Elsevier Ltd. All rights reserved.

* Corresponding author.
  E-mail address: mabdelhamid@ucmerced.edu (M. Abdelhamid).

1. Introduction

Hybrid solar photovoltaic thermal (PV/T) systems have long been proposed as an effective means of improving system performance by using a combination of PV devices and thermal collectors to produce both heat and electricity [1]. The most common PV/T systems use air [2,3] or water [4,5] as the heat transfer fluid (HTF) inside flat plate collectors. The authors in [6] performed an extensive study on water and air cooling PV/T systems, while in [7,8] extensive studies of different flat plate PV/T collectors are reported. All of these designs, however, are limited to low temperatures applications. Other concentrating CPV/T systems have been developed to meet the higher temperatures required by other solar applications, [9,10]. The authors in [10] reported on the ANU-Chromasun MCT prototype which is a Fresnel collector that has an average 8% electrical efficiency and average thermal efficiency of 50% under 10X concentration. The use of non-imaging optics with CPV/T has also received some attention [11,12]. In [11] the authors reported on a water-cooled PV/T system with a low concentration ratio 4X using compound parabolic concentrators (CPC), with a maximum fluid temperature of around 65 °C. In [12], the concentrator was designed using Fresnel lenses and flat mirrors with crystalline silicon cells to get a uniform irradiation on the solar cells. A novel air-gap-lens-walled CPC incorporated with PV/T system is reported in [13–16], which has the electrical and thermal efficiencies of 6.0% and 35.0% respectively with an output water temperature of 70 °C. Apart from the HTF and concentration ability, the performance of a PV/T system depends on the type of solar cell as well. Common PV/T systems use crystalline silicon solar cells or thin film PV types such as amorphous silicon [17]. Crystalline silicon solar cells are more efficient, however they are affected much more negatively by raising their working temperatures compared to thin film PV [18–20].

As extensively reviewed in [21–28], there has been no work in the field of medium to high concentration PV/T collectors operating at high temperature due to the system complexity added by cooling mechanisms, tracking capability, and solar cell performance. The CHAPS system [21], however, consists of glass-on-metal mirrors that focus light onto Mono-Si solar cells with a geometric concentration ratio of 37X using water. It reaches a fluid outlet temperature of 80 °C. In addition, the use of high efficiency solar cells such as Gallium Arsenide (GaAs) in PV/T devices has rarely been investigated in the literature, despite the fact that GaAs cells have better efficiencies and temperature coefficients than other conventional solar cells under high concentration PV/T systems [29].

In this work, we report on the design, simulation, fabrication, and experimental testing of a novel double-stage high-concentrated hybrid PV/T solar collector. The system is novel in the following regards. By optically coupling the PV and thermal components, they can each independently achieve their optimized working temperature. The addition of a secondary nonimaging concentrator enables the thermal component to reach a 60× concentration ratio and high operating temperatures, and the system exergy efficiency is maximized by using the solar cells as specular mirrors for lower energy photons.

2. Design of hybrid PV/T system

2.1. Optical theory

The proposed optical system uses a two stage concentrator (see Fig. 1). Optimization of the primary and secondary concentrators is based on the half rim angle (ϕ) of the system (Eqs. (1)–(5)) [30].
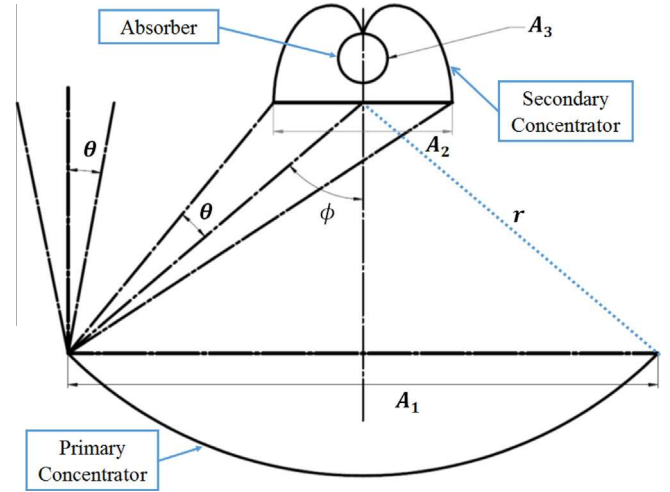

Fig. 1. Double stage concentrator of the proposed optic design.

$$C_{1st} = \frac{A_1}{A_2} \tag{1}$$

$$C_{2nd} = \frac{A_2}{A_3} \tag{2}$$

$$C_{1st} \leqslant \frac{2r \sin \phi}{\frac{2r\theta}{\cos \phi}} = \frac{(\sin \phi \cos \phi)}{\theta} \tag{3}$$

$$C_{2nd} \leqslant \frac{1}{\sin \phi} \tag{4}$$

$$C = C_{1st} \cdot C_{2nd} = \frac{\cos \phi}{\theta} \tag{5}$$

where

C: Final concentration ratio of the system
C_{1st}: Primary concentrator ratio
C_{2nd}: Secondary concentrator ratio
θ: Acceptance angle [°]
A_1: Primary concentrator aperture area [m^2]
A_2: Secondary concentrator aperture area [m^2]
A_3: Absorber area [m^2]
r: Radius [m], which is focal length

The closer ϕ is to 0°, the closer the concentration ratio is to theoretical maximum. A 0° ϕ, however, results in an infinitely long focus length with a flat surface as the primary reflector. The secondary concentrator in this case will also be infinitely long. Due to practical considerations we chose $\phi = 45°$, which reaches about 70% of the ideal concentration.

2.2. Proposed design

The main components of the proposed system are the (i) primary parabolic concentrator and (ii) hybrid PV/T receiver (Fig. 2). The receiver includes a nonimaging compound parabolic concentrator (CPC) which provides secondary concentration to the high temperature thermal absorber. The receiver is made of several sub-components including (a) aluminum minichannel struts, which roughly approximate the "wings" of the CPC and serve as fluid channels to provide active cooling of the cells, (b) thin film GaAs cells which are applied directly to the aluminum minichannels, (c) curved mirrors to form the involute portion of the CPC, (d) selectively coated absorber which receives concentrated light from the CPC and serves as the high temperature (400 °C) fluid
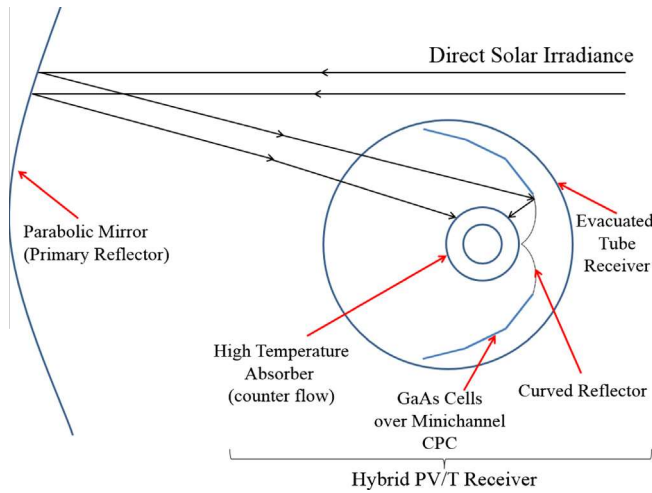
Fig. 2. Hybrid PV/T collector schematic.

channel, (e) outer glass tube which allows the entire receiver to be evacuated for heat loss reduction.

2.3. Principle of operation

The parabolic mirror (primary concentrator) reflects and focuses incoming direct beam solar irradiance toward the hybrid PV/T receiver and as this light passes through the glass tube enclosure it strikes either (a) the GaAs covered minichannels, (b) the curved involute mirror portion of the CPC, or (c) the high temperature absorber directly. Light that strikes the GaAs cells is spectrally split based on the 870 nm bandgap cutoff, with about 90% of photons with energy higher than the bandgap being absorbed and converted to electricity or heat, and about 92% of photons with energy lower than the bandgap being reflected towards the high temperature absorber. Thus the system produces electricity directly from the PV cells. The high temperature absorber receives the spectrally split light reflected from the GaAs cells as well as light reflected from the curved mirror involute portion of the CPC and light that strikes the absorber from the primary parabolic mirror directly.

2.4. System components

2.4.1. Primary parabolic concentrator

The primary parabolic mirror structure was constructed out of wood and the mirror surface was formed by a flat plastic laminate over which the highly reflective silver film ReflecTech [31] was applied. The mirror characteristics are tabulated in Table 1. The aperture area of the primary parabolic mirror (A_1) is 5 m². The receiver tube is located at the focus (distance r from the mirror surface, See Fig. 1). The acceptance angle (θ) and the primary

Table 1
Primary parabolic mirror characteristics.

Characteristic	Quantity
Aperture area (A_1)	5.0 m²
Aperture width	5.0 m
Aperture length	1.0 m
Focal length (r)	3.02 m
Half rim angle (ϕ)	45°
Acceptance angle (θ)	0.6°
Primary concentration ratio (C_{1st})	45
Reflectance	93%

concentration ratio (C_{1st}) are discussed in following sub-sections. Standard parabolic mirrors generally use a half rim angle (ϕ) of 90° to maximize illumination of the absorber surface. Since we are using a secondary concentrator, which evenly illuminates the entire absorber surface area (A_3), we employ $\phi = 45°$ so that the secondary concentrator is still able to provide additional concentration. The reflectance of the mirror is 93% based on measured reflectance data of ReflecTech [31].

2.4.2. Hybrid PV/T receiver

The design of the hybrid PV/T receiver, as illustrated in Fig. 3(a), is based on nonimaging optics and previous work on inserted internal CPC reflectors [32]. Standard parabolic troughs (see Fig. 3(b)) generally use a 70 mm diameter absorber [33], however, the angular potential of the surface is not fully utilized. This is effectively wasted surface and a standard parabolic trough system focusing from 5 m to a 70 mm diameter tube will only reach concentration ratios ~23×. This problem is solved using a secondary concentrator as the CPC illuminates the entire surface of a smaller diameter absorber.

The CPC was truncated to fit within a 120 mm inner diameter glass tube. A truncation to 94% of the original aperture width of the CPC allowed a reduction to 66% of the original height allowing it to fit nicely within the glass tube. The CPC was approximated using flat minichannel segments. This approximation led to a 91% optical efficiency compared to an ideal CPC as will be discussed later. Table 2 shows the main PV/T CPC receiver specifications

The system geometric concentration ratio (C) is calculated based on the proposed design specifications (Eqs. (6)–(8)) of approximately 60×, which allows it to operate at similar or even higher temperatures compared to conventional parabolic trough systems even under partial utilization of the solar spectrum.

$$C_{1st} = \frac{A_1}{A_2} = \frac{5000 \text{ mm}}{111.12 \text{ mm}} = 45\times \tag{6}$$

$$C_{2nd} = \frac{A_2}{A_3} = \frac{111.12 \text{ mm}}{\pi * 26.7 \text{ mm}} = 1.324\times \tag{7}$$

$$C = C_{1st} \cdot C_{2nd} = 59.6\times \tag{8}$$

Here, C_{1st} is the ratio between the primary parabolic to CPC aperture, C_{2nd} is the ratio between the apertures of the CPC to the absorber, A_1 is the aperture area of the parabolic mirror, A_2 is CPC aperture area, and A_3 is the absorber area.

2.4.3. GaAs solar cell

The solar cells used in the design are state-of-the-art single junction GaAs cells manufactured by Alta Devices. Because of their sharp bandgap cutoff at 870 nm with 90% absorption at sub-bandgap wavelengths and 92% reflectance at wavelengths above the bandgap as shown in Fig. 4, they are also very efficient spectrally selective reflectors. The solar to electric efficiency of these cells is 28.8% at room temperature with a temperature coefficient of −0.08% per C [34]. In the proposed design the GaAs cells occupy only 2.4% of A_1, allowing the system to be more affordable, while still receiving 41.6% of the incoming direct beam irradiance incident on the trough. The solar cells serve two purposes; spectral splitter/concentrators = and electricity generation.

2.4.4. Minichannels and curved involute mirror

The wings of the CPC are approximated by three 20 mm (~0.79 in.) long segments of minichannels. The design of minichannels is shown in Fig. 5(a). They serve as the structure onto which the GaAs cells are applied as well as allowing for active cooling of the cells to control their temperature. The involute portion of the CPC is formed from Alanod Miro-Sun which has a total solar reflectance of approximately 89% [35]. The curved involute mirror
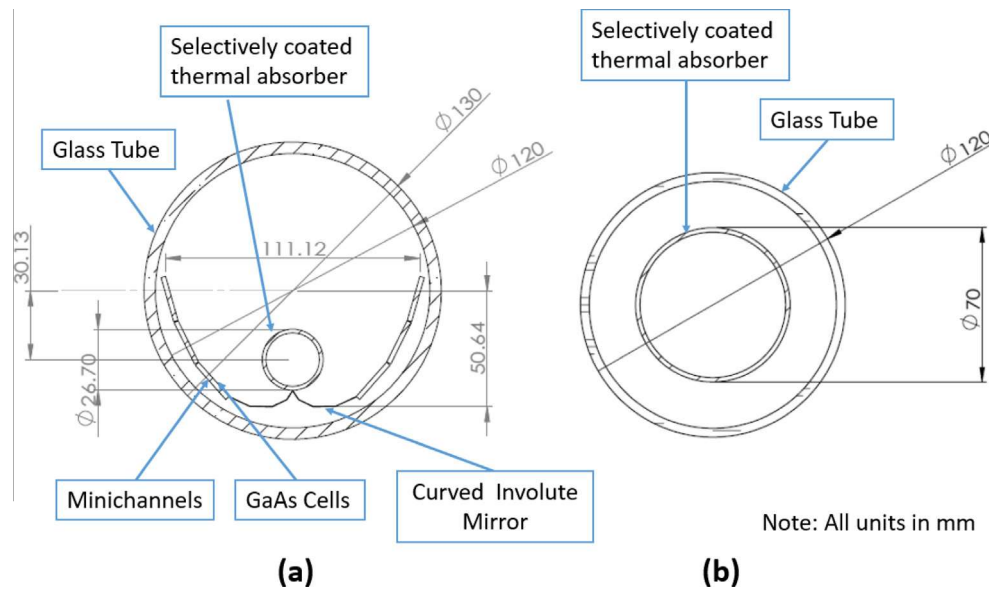
Fig. 3. (a) Hybrid PV/T receiver (b) Standard receiver.

Table 2
Secondary CPC specifications.

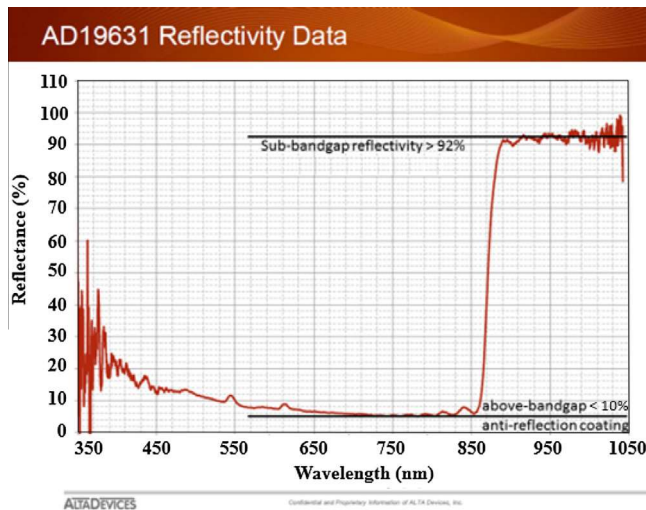| PV/T receiver CPC specifications	Quantity
Secondary acceptance angle, which is same as ϕ	45°
Absorber outer diameter	26.7 mm
CPC truncation by height	66%
CPC truncation by aperture	94%
Truncated aperture width	111 mm
Secondary concentrator ratio (C_{2nd})	1.32
Optical efficiency compared to ideal CPC	91%

Fig. 4. Spectral reflectance of Alta Devices' state-of-the-art GaAs cells.

and the minichannels integrated into the PV/T receiver design as shown in Fig. 3(a). The minichannels shape was supported by 4 braces along the length of the tube (see Fig. 5(b)).

2.4.5. High temperature absorber

The high temperature absorber was constructed of 3/4″ Schedule 5 stainless steel with an outer diameter of 26.7 mm. It was selectively coated by Himin, which has greater than 95% solar

weighted absorption and approximately 0.08 emissivity at 300 °C [36]. The glass tube was capped with a stainless steel cap (see Fig. 5c), which was clamped externally to the glass tube. The stainless steel cap had an inlet for the vacuum system, counter flow inlet and outlet for the high temperature thermal fluid, inlet and outlet for the cooling stream through the minichannels, and a vacuum feed-through for the solar cell electrical leads to pass through.

3. System performance

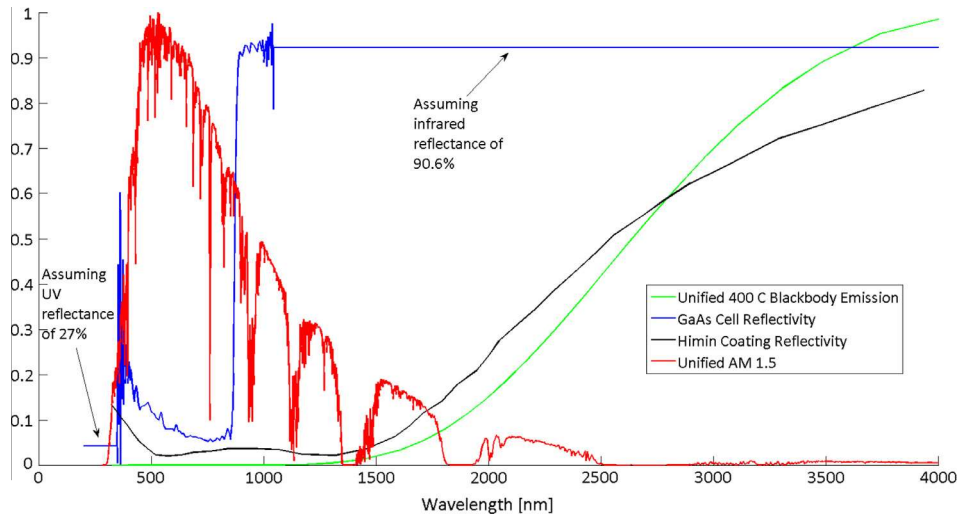### 3.1. Optical performance model

An optical model include all spectral surface properties of system components was developed and analysis was performed using ray tracing software. The reflectance of GaAs cell in the infrared region was assumed constant by extrapolation of the reflectance of the longest wavelength measured (see Fig. 6).

Virtual receivers were set at the aperture of the secondary concentrator, the solar cells; and the selective absorber to determine optical throughput at these key points in the system. Analysis of the CPC shows an efficiency of 91% compared to an ideal CPC (see Fig. 7(a)) due to truncation and the approximation of the curve by flat minichannel segments.

Optical modeling of the complete system was simulated using uniformly distributed rays within 0.8° for acceptance angle (off-axis angles) as shown in Fig. 7(b). Of the total incoming irradiance to the system, 82% is incident on the aperture of the 2nd concentrator (losses from reflection and glass transmittance). 42% of the total incoming irradiance is directly incident on the solar cells, with 26% being either converted to electricity or absorbed as heat. 15% of the total light from the sun is incident on the curved involute mirror, out of which 1% is absorbed. 50% of the total incoming energy reaches the selective absorber (coming from light reflected directly by the parabolic mirror as well as reflection of both the solar cells and the curved involute mirrors) out of which 47% is absorbed. The optical model generates three key performance parameters that are used to calculate thermal performance: radiation absorbed by the absorber (G_{abs}), radiation incident on the GaAs cells ($G_{cell\_Inc.}$), and the amount of radiation absorbed by the GaAs cells (G_{cell_abs}).
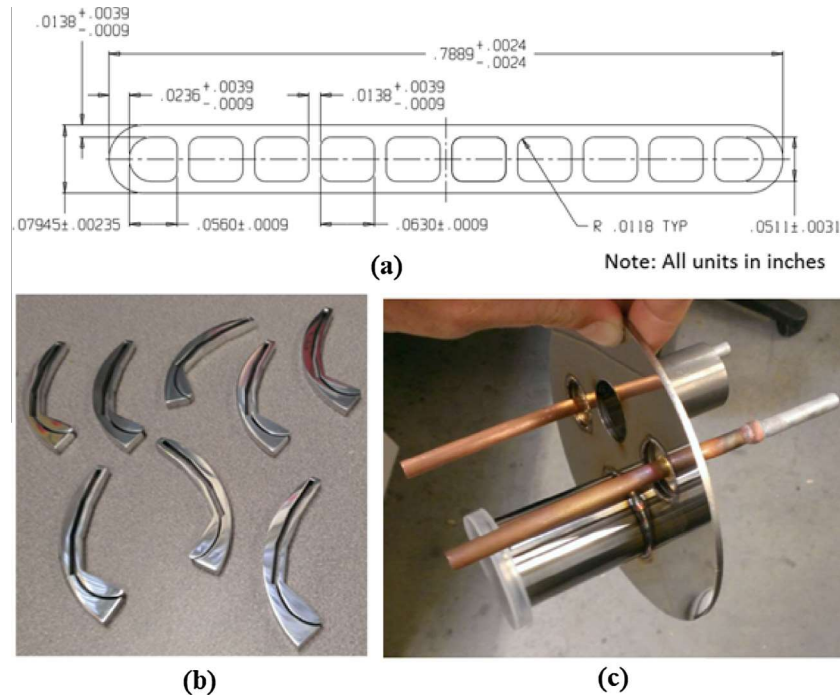
Fig. 5. (a) Minichannel design; (b) minichannel support braces; (c) receiver end cap with ports for HT thermal cooling, evacuation, and electrical connections.

Fig. 6. GaAs cell and Himin coating reflectivity vs. blackbody emission and AM_1.

3.2. Thermal performance model

Heat transfer through the high temperature counter-flow absorber tube is determined by a finite element analysis model using the absorbed radiation input from the optical model. The model includes a radiation balance between the hot absorber surface and the inside of the glass vacuum tube. For simplicity, it was assumed the GaAs cells would not absorb any of the re-radiation from the absorber because they are highly reflective in the infrared region. Table 3 shows the thermal performance model parameters used.

The model determines the outlet temperature of the high temperature fluid stream based on a set input temperature, flow rate, and direct beam solar irradiance to the system. Heat loss from the receiver end cap was incorporated into our model

and the thermal output ($Q_{high\ temperature\ stream}$) is calculated using Eq. (9).

$$Q_{high\ temperature\ stream} = \dot{m}c_p(T_{out} - T_{in}) \tag{9}$$

where

$\dot{m}$: Mass flow rate of fluid [kg/s]
c_p: Heat capacity of fluid [kJ/kg K]
T_{out}: Outlet temperature of fluid stream [°C]
T_{in}: Inlet temperature of fluid stream [°C]

The temperature coefficient of the GaAs cells is well documented [34] and their solar to electric efficiency(η_{GaAs}) is calculated based on cell operating temperature (T_{cell}) in °C using Eq. (10).
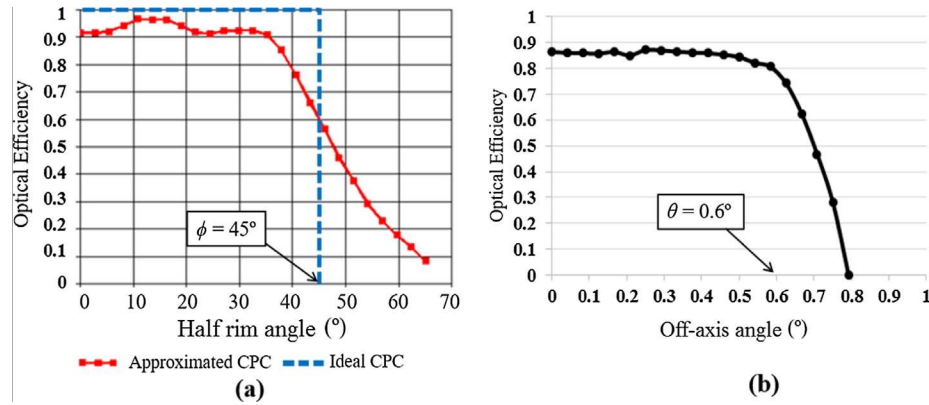
Fig. 7. (a) Optical efficiency with half rim angle of approximated CPC compared to ideal CPC; (b) system optical performance with off-axis angle.

Table 3
Thermal performance model parameters.

Thermal model parameters	Value
Emissivity of selective coating at 300°C	0.08
Emissivity of GaAs cell	0.10
Emissivity of aluminum minichannels	0.08
Thermal conductivity of stainless steel	20 W/m K
Absorptivity of glass in infrared region	100%

$$\eta_{GaAs} = 0.308 - 0.0008 \cdot T_{cell} \tag{10}$$

Total electric output of the system (Q_{GaAs}) is calculated based on the amount of radiation incident ($G_{cell\_Inc.}$) upon the cells as determined by the optical model using Eq. (11).

$$Q_{GaAs} = \eta_{GaAs} \cdot G_{cell\_Inc.} \tag{11}$$

Energy efficiency from the high temperature streams (η_{energy}) is calculated as per Eq. (12).

$$\eta_{energy} = \frac{\dot{m}c_p(T_{out} - T_{in})}{G} \tag{12}$$

4. Experimental setup and hybrid PV/T prototype

The experiment was performed at University of California Merced's Castle Research Center. The latitude and longitude for the location are 37.3 °N, and 120.6 °W, respectively. The data analyzed in this article was collected from March 9, 2015 to March 27, 2015.

4.1. Solar and environmental sensors

Different state variables are measured for the purpose of system performance evaluation and safety considerations, including solar radiation, ambient temperature, flow rate, pressure, and fluid temperature. There were a total of 24 sensors installed to measure these variables, including: two electromagnetic volume flow rate sensors; one Coriolis mass flow meter; eighteen thermocouple sensors; one normal incidence pyrheliometer (NIP); and one precision spectral pyranometer (PSP). The measurements collected from these devices were used to characterize the system performance. The data is collected at 5 s intervals. Fig. 8 shows the main sensors at the research facility and Table 4 lists the type and specification of sensors used in the solar and environmental testing rig for each measurement of interest. Direct normal irradiance (DNI) and global horizontal solar irradiance (GHI) were measured using mounted normal incidence pyrheliometer and precision spectral pyranometer, respectively. The ambient temperature was measured using a

K-type thermocouple inside a radiation shield. The fluid temperature was measured by heavy duty K-type thermocouple sensors where a clusters of three sensors used at inlet and outlet of receiver. The mass flow rate was measured by Coriolis mass flow meter.

4.2. Hybrid PV/T receiver prototype

The GaAs PV cells were applied onto a thin aluminum plate and glued to the minichannels with a thermally conducting yet electrically isolating thermal paste (Omega-Therm). Fig. 9 shows the actual parabolic trough reflector and the hybrid PV/T receiver.

4.3. High temperature loop

The high temperature loop was constructed from schedule 80 stainless steel and all plumbing was socket welded, except for main components, which were secured with 300 class flanges. The pressure required to keep Therminol VP-1 in a liquid state at 400 °C is approximately 170 psi (1.17 MPa). Pressure was applied by nitrogen from a nitrogen tank via the expansion tank which also blanketed the system to prevent oxidation of the oil at elevated temperatures. Therminol VP-1 crystallizes at 12 °C (54 F) and since the loop was constructed outdoors and would be exposed to low ambient temperatures during the winter, it was designed so that its entire volume could be drained into a storage tank at the end of the day. The drain-back tank contained an immersion heater that allowed us to pre-heat the oil above 100 °C prior to charging the system. The high temperature loop design is shown in Fig. 10.

The system was designed for a flow rate of 50 g/s, or about 1 gallon per minute. At this flow rate, the oil was expected to rise by 10 °C through the solar collector (at 400 °C and 800 W/m² DNI). This was chosen to reduce thermocouple inaccuracy. The fluid was connected to the dual axis tracker via flexible hose and to the receiver along the bottom of the aluminum support trusses. At the inlet and outlet of the receiver a cluster of three thermocouples was installed in the flow path to accurately measure the temperature rise of the heat transfer fluid across the receiver. The setup of the high temperature loop is shown in Fig. 11.

4.4. Cooling loop

The fluid used for cooling the cells was Duratherm 600. It was circulated by a Chromalox micro-Therm oil temperature control system. Flowrate was measured by another Coriolis mass flow meter and temperature was measured via thermocouple clusters positioned as close as possible to the inlet and outlet connections at the receiver.
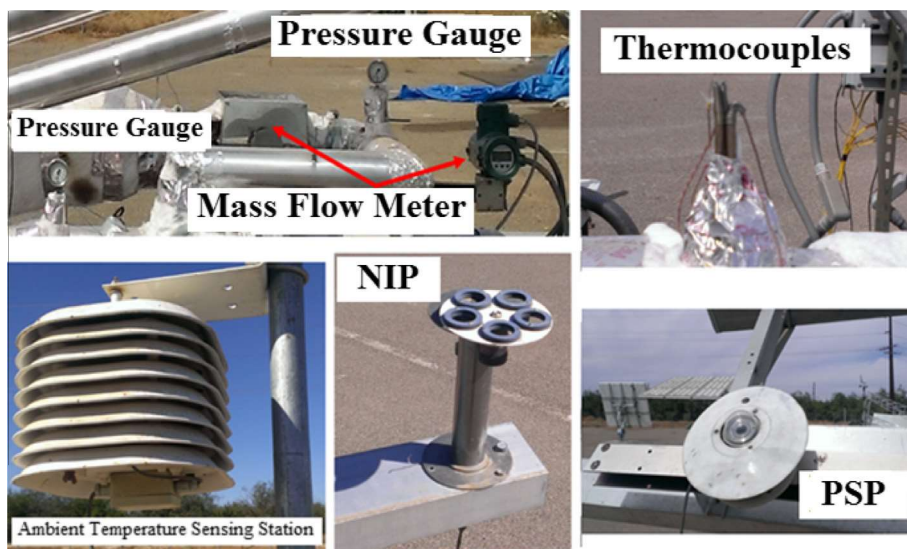
Fig. 8. Solar and environmental sensors in testing facility.

Table 4
Measurements, type and specification of sensors.

| Measurements	Quantity	Sensor	Calibration range	Instrument uncertainty	Manufacturer
Ambient temperature	1	Thermocouple, Type k	Up to 1335 °C	Less than 2.8 °C in 25 week	Omega [37]
System Pressure	2	Pressure Gauge	15,000 psi	±1% full scale	Ashcroft [38]
Fluid temperature	18	Thermocouple, Type k	Up to 1335 °C	Less than 2.8 °C in 25 week	Omega [37]
Mass flow rate	1	Coriolis mass flow meter	0–7 gallon/minute	0.35–0.38% of rate	Yokogawa Corporation of America [39]
Direct normal irradiance (DNI)	1	Normal Incidence Pyrheliometer	Field of View 5° and sensitivity approx. 8 μV/W m^{-2}	Less than 1%	The Eppley Laboratory, INC. [40]
Global horizontal solar irradiance	1	Precision Spectral Pyranometer	Approx. 8 μV/Wm^{-2} 0–2000 W/m^2	Less than 1%	The Eppley Laboratory, INC. [40]
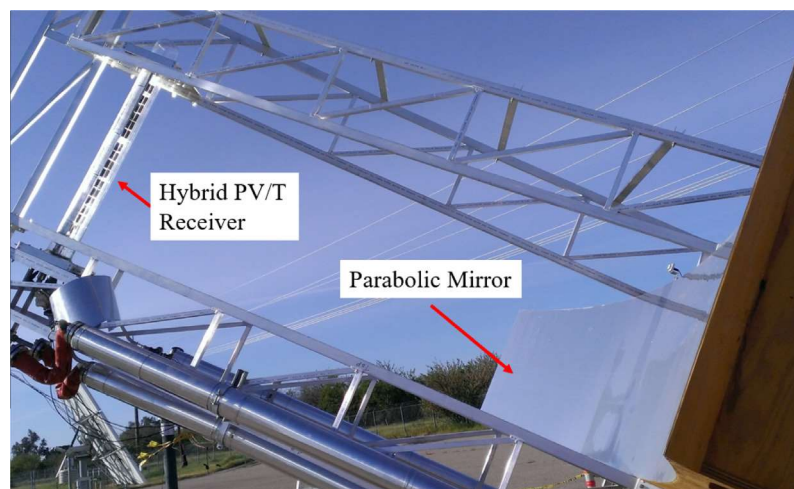
Fig. 9. Parabolic mirror and hybrid PV/T receiver.

5. Results and discussions

5.1. High temperature thermal tests

Tests were conducted under a variety of solar and environmental conditions ranging from low to high DNI and at outlet temperatures of the high temperature stream from 60 °C to 365 °C. The results are summarized in Figs. 12 and 13. Fig. 12(a) shows the DNI and flow rate for each of the tests. The high temperature absorber outlet temperature, ambient temperature, and thermal efficiency are shown in Fig 12(b).

Fig 13 shows the experimental results compared to the simulated results of all high temperature thermal tests with respect to outlet temperature. On average the thermal efficiency of the
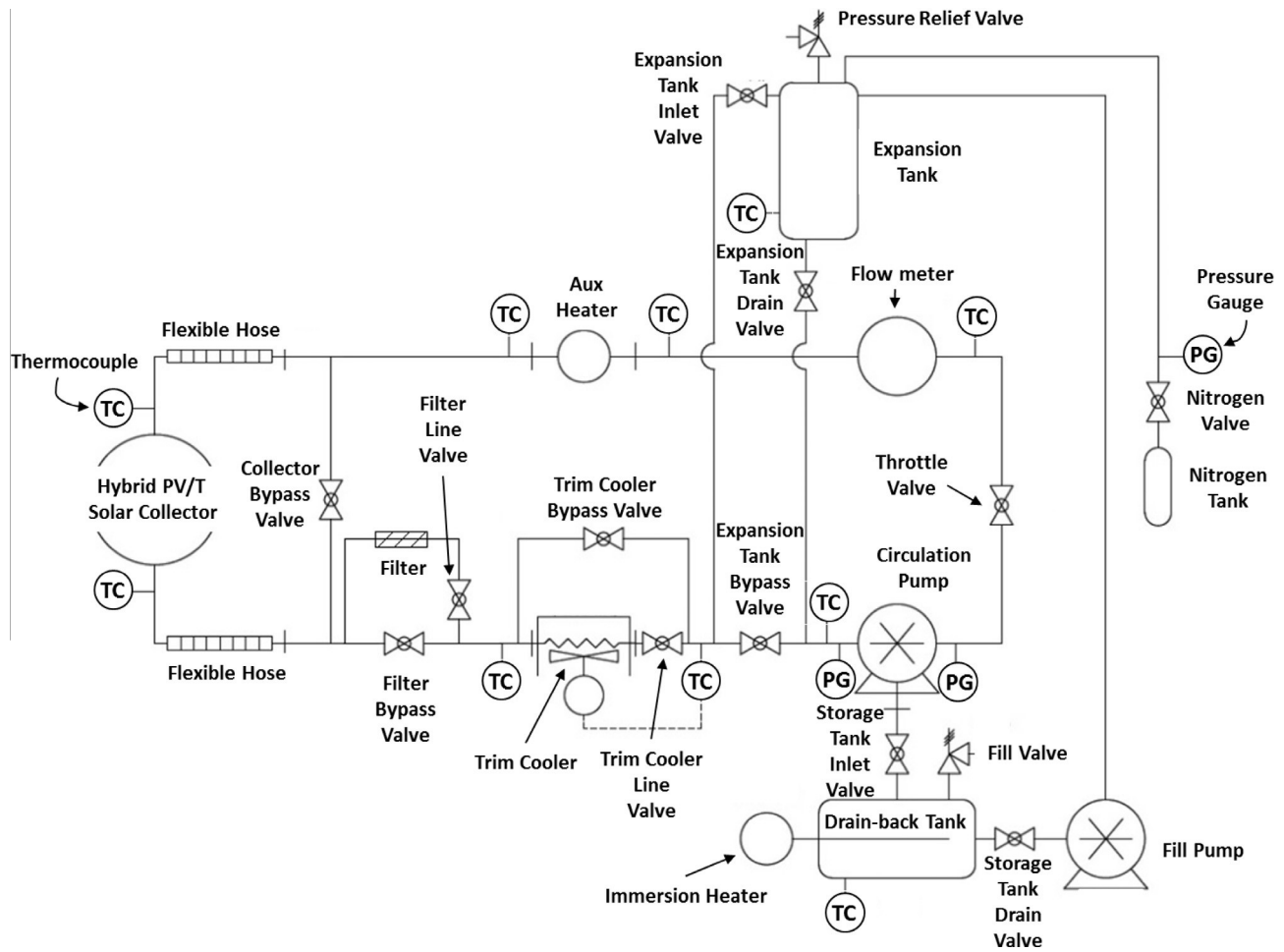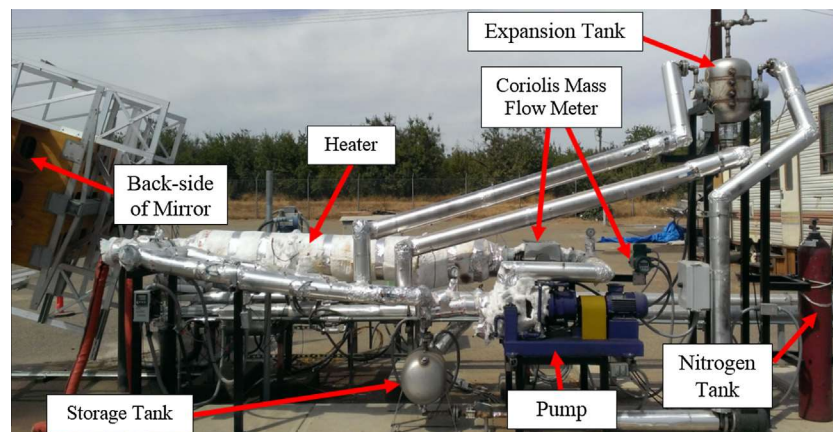
Fig. 10. High temperature loop design.

Fig. 11. High temperature loop setup.

experiment is around 37%, lower than the 47% efficiency predicted by the model. We discuss causes for the lower than expected efficiency in Section 5.3.

5.2. PV electrical efficiency

The best direct electrical efficiency data we obtained was on March 20th under highly cloudy conditions. The output voltage of the PV cell was measured and electrical efficiency calculated

and the results are shown in Fig. 14. The maximum solar electrical efficiency was around 8% compared to 9% simulated result, the short circuit current (I_{sc}) was 230 mA and the fill factor (FF) was determined to be 84.3%.

5.3. Experimental limitations and issues

The first issue we faced was the failure of the elevation actuator on our tracker during the experiment. Because of this, we could
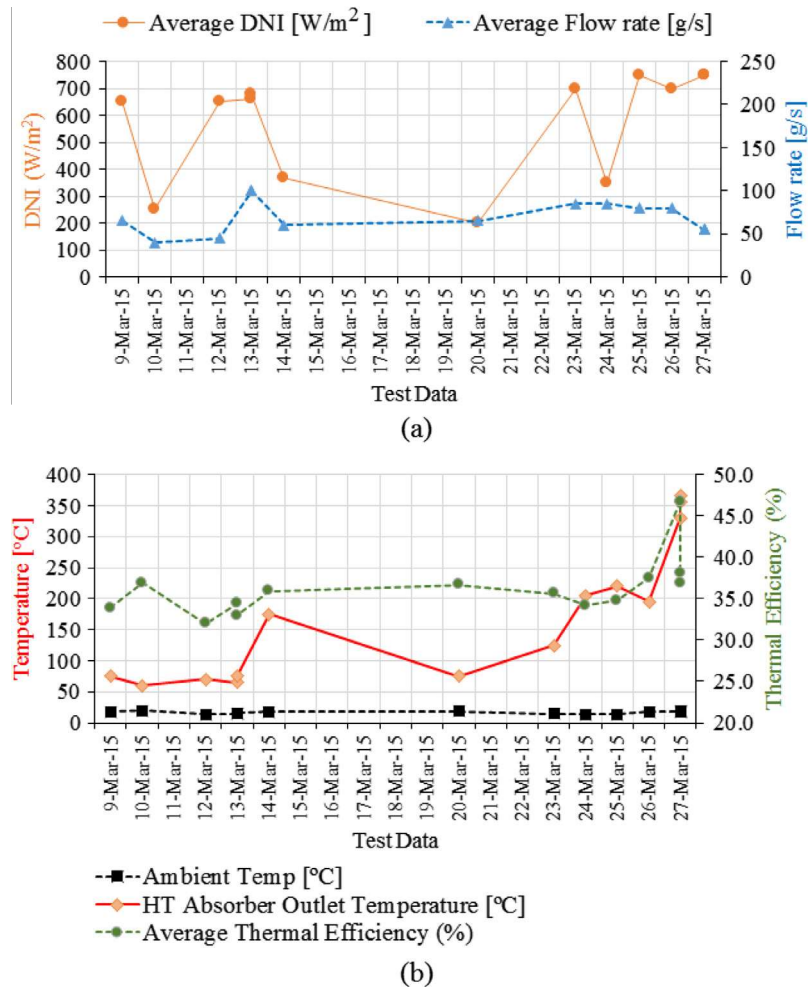
Fig. 12. Experimental input and results (a) average DNI and flow rate, (b) high temperature absorber outlet temperature and thermal efficiency.
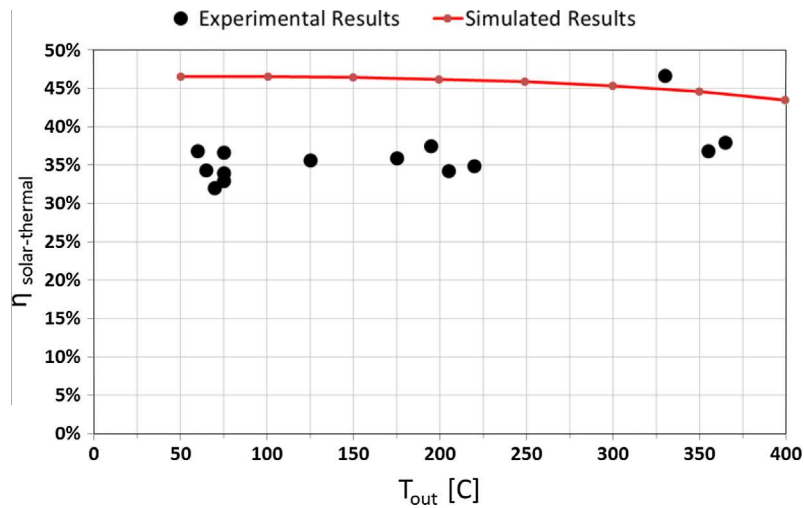

Fig. 13. Solar thermal efficiency results.

only get full illumination of the receiver tube at a specific time in the morning each day. Subsequent tests only saw partial illumination due to increased sun angle. To account for this, all thermal power and efficiency calculations are elevation corrected to normalize to full illumination of the receiver tube (measured thermal output is divided by measured percentage of tube length that is illuminated).

The second issue we discovered was our methods for both attaching the cells to the minichannel substrate using Omega Therm and soldering the electrical leads to the cells were not as
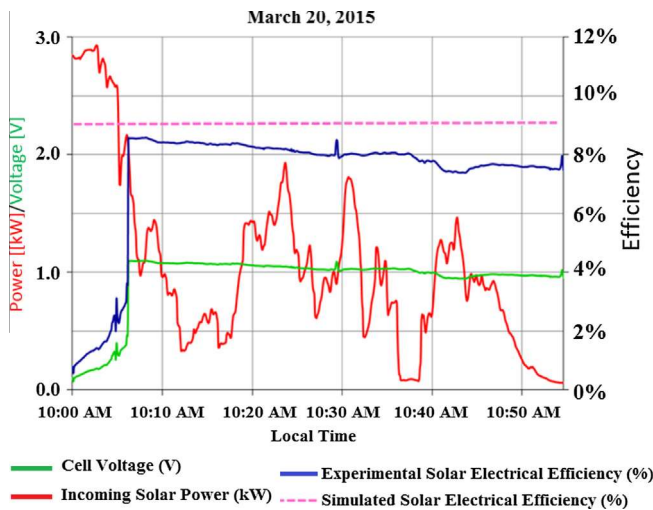
Fig. 14. Solar electrical efficiency.

robust as desired. The adhesive properties of the paste were lost after extended evacuation and heating and we had to tie down each cell individually with enameled wire to hold them in place.

Another major problem we had was the inability to pull a strong vacuum (E^{-5} mbar) due to leaks in the vacuum connections, leaks in internal tube assembly, and outgassing. Just outside the receiver cap we measured a vacuum as low as $2.2\,E^{-2}$ mbar, but still had condensation inside the glass tube. This indicates a source of error in our vacuum measurement as we were not actually measuring the vacuum inside the tube. To account for heat loss caused by an inadequate vacuum we corrected all the high temperature thermal efficiencies. Heat loss measured from the absorber at temperature prior to the test is added to the thermal gain during test to adjust to zero net heat loss. As a result of these corrections, the efficiency vs. temperature graph in Fig. 13 is flat and does not decrease with temperature as one would expect in a perfect evacuated system due to radiative loss. In fact, due to these corrections, our efficiencies in Fig. 13 are simply measurements of the optical efficiency. The condensation formed on the inside of the glass tube caused a significant amount of reflection/scattering, preventing light from entering the receiver tube. Over time the condensation in the glass tube slowly cooked out due to high test temperatures.

We attribute the clearing up of the condensation with the slight increase in efficiency with temperature as shown in Fig. 13 (we tested the highest temperatures last). Another source of error present in all solar systems is dusting of reflective surfaces. Lastly, the 47% efficiency at 330 °C (see Fig. 13) is sort of an anomaly. We have looked at the data for that test and there is no clear reason (solar and flow rate were very stable) for the increased efficiency. The data is included for completeness.

6. Annual performance and cost analysis

The annual average system performance over an average hourly year using average DNI information from NREL's National Solar Radiation Data Base (NSRDB) [41] for Merced, California is estimated. Fig. 15 shows the average annual DNI at Merced, CA with maximum DNI at noon is around 600 W/m². Assuming the presented PV/T system is used for electricity generation, where the high temperature stream runs Steam Rankine turbine with typical efficiency of 37.5% at about 400 °C [42]. The annual hourly average estimated generated electricity per system aperture area (W/m²) is shown in Fig. 15. Here, the total electricity generation is the summation of direct electricity generated by GaAs solar cells and electricity generated by Steam Rankine turbine runs by our high temperature thermal stream. This mean at noon in Merced, CA, when the DNI is equal 600 W/m², the total electricity generation is around 148 W/m² (total around 25%).

The cost is estimated for the installed hybrid solar system per unit of parabolic trough aperture area ($/m²) using a bottom–up approach as $283/m² as shown in Table 5 including all solar field materials, labor installation, and assembly. Our analysis is based on the baseline cost for parabolic trough solar fields in the United States within U.S Department of Energy NREL's System Advisor Model (SAM) [43,44]. The cost of GaAs single junction cells with 29% efficiency is based on NREL's long-term estimation [45].

7. Conclusion and future work

A novel double-stage high-concentration PV/T hybrid solar system has been developed [46] to simultaneously generate electricity and high temperature dispatchable heat. In this paper, we presented the details of our design, modeling, experimental setup, procedure, fabricated prototype, performance results, and an economic analysis of the system.
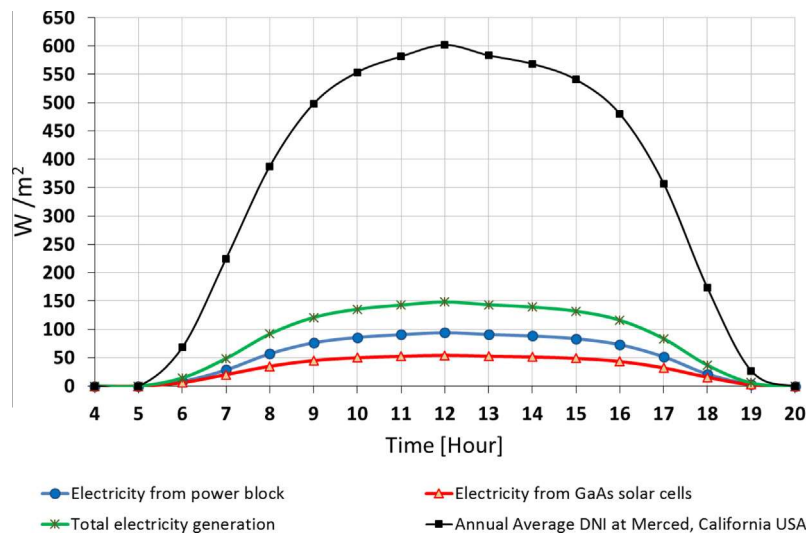

Fig. 15. Average annual hourly DNI at Merced, CA (source data [41]) and annual hourly average PV/T system electricity generated per system aperture area (W/m²).

Table 5
Estimation cost of the proposed PV/T system.

Component	Cost ($/m^2)[a]	Description/justification
Mirror modules	16.12	Based on commercial data
Sun tracker	3.74	SAM
Foundation and support structure	17.93	SAM
Instrument and control	7.95	SAM
Electrical	3.14	SAM
Fabrication tent	1.24	SAM
Collector frames	20.0	Based on commercial data
Absorber tube, glass tube and fitting	28.3	Based on commercial data
Solar collector assembly Misc. components	2.0	SAM
GaAs thin film cell on mini-channel structure	22.27	Estimation based on mass produced 29% single junction GaAs price of $2.4/W, which still is much higher than Sunshot estimation $0.5/W [45]
Minichannels	2.0	Based on commercial data
Adhesive	1.49	Based on commercial data
Piping	34.44	SAM
Heat transfer fluid	22.45	SAM
Pumps	5.69	SAM
Expansion system	6.60	SAM
Labor installation	62.0	SAM
Subtotal cost ($/m^2)	257.36	Added all the above
Assembly cost ($/m^2)	25.73	10% of total cost
Total cost ($/m^2)	283.10	Subtotal cost plus assembly cost

[a] Cost is per unit of parabolic trough aperture area.

The two-stage hybrid concentrator uses a 5 m^2 parabolic trough to focus sunlight towards a secondary CPC to produce electricity from high efficiency thin film single junction GaAs solar cells together with high temperature thermal energy. The GaAs cells are part of a wide angle secondary concentrator and generate electricity directly while also providing additional concentration towards the high temperature absorber by reflecting sub-bandgap photons. The spectrally selective reflectivity of the GaAs is used to maximize the exergy output of the system. In addition, through this design we optically coupling the photovoltaic component and the thermal component so they can independently achieve their optimized working temperatures in vacuum. This unique design achieves ~60× concentration ratio from parabolic aperture to high temperature absorber, which is significantly higher than conventional CPV/T systems. This helps the thermal absorber to achieve higher temperatures (365C) even under partial utilization of the solar spectrum allowing the PV/T technology to reach the higher temperatures required by alternative solar applications (e.g., power generation). A conventional hybrid PV/T receiver would not be able to achieve such temperatures, resulting in a low power block efficiency, and typical solar cells would particularly suffer from elevated temperatures.

Experiments were conducted during March 2015 at the University of California Merced's Castle Research Center under a variety of solar and environmental conditions ranging from low to high DNI and we are able to prove the concept by simultaneously generating electricity from the PV cells and dispatchable high temperature thermal energy from the remaining solar energy. Due to the properties of Therminol VP-1, we were only able to reach a maximum outlet temperature of 365 °C. On average, the high temperature thermal efficiency of the experiment was around 37% which is lower than the 47% efficiency predicted by the model. The maximum electrical efficiency was found to be around 8%, which has room for improvement in future work. The main reasons for the differences between the experimental results and the model

output are imperfections of the prototype receiver tube (i.e., cell attachment mechanism, leaks in the vacuum connections, leaks in internal tube assembly, outgassing, formation of condensation), problems with the dual axis tracker, and imperfections in the primary mirror.

The maximum total system electricity generation is estimated around 25% of the incoming DNI by assuming the solar energy is converted directly to electricity by GaAs cells and the thermal energy is run through a steam turbine for electricity generation. From the perspective of the potential of electricity generation, the design can be optimized for the centralized utility solar field to have both dispatchable (thermal storage) and instantaneous electricity generation. Whereas the conventional CPV/T system can only harvest electricity from the PV component, and at best, co-generate low quality heat. Such a heat has no potential for electricity generation, similar to the waste heat from the fossil fuel plants.

The installed hybrid PV/T solar system cost per unit of parabolic trough aperture area is estimated at $283/m^2, including all solar field materials, installation labor, and assembly cost. The combination of a high concentration ratio and state-of-the-art GaAs thin film solar cells allows the system to be efficient and economic. By collecting as much solar energy as we can, this design has a significantly improved exergy output compared to existing parabolic trough plants. Future work includes replacing the heat transfer fluid with a novel material that will allow us to reach higher temperatures [47], as well as developing better methods for manufacturing and assembling the receiver (e.g., cell attachment mechanism, better vacuum quality). All of these improvements are currently being implemented in our new project funded by the U.S Department of Energy.

Acknowledgements

References

[1] Kern Jr EC, Russell MC. Combined photovoltaic and thermal hybrid collector systems. In: 13th IEEE Photovolt. Spec., Washington, DC, USA: Massachusetts Inst. of Tech., Lexington (USA). Lincoln Lab.; 1978. p. COO – 4577–3; CONF – 780619–24.

[2] Aste N, Chiesa G, Verri F. Design, development and performance monitoring of a photovoltaic-thermal (PVT) air collector. Renew Energy 2008;33:914–27. http://dx.doi.org/10.1016/j.renene.2007.06.022.

[3] Kumar R, Rosen Ma. A critical review of photovoltaic-thermal solar collectors for air heating. Appl Energy 2011;88:3603–14. http://dx.doi.org/10.1016/j.apenergy.2011.04.04.

[4] Aste N, del Pero C, Leonforte F. Water flat plate PV-thermal collectors: a review. Sol Energy 2014;102:98–115. http://dx.doi.org/10.1016/j.solener.2014.01.025.

[5] Chow TT, Chan ALS, Fong KF, Lin Z, He W, Ji J. Annual performance of building-integrated photovoltaic/water heating system for warm climate application. Appl Energy 2009;86:689–96.

[6] Tripanagnostopoulos Y, Nousia TH, Souliotis M, Yianoulis P. Hybrid photovoltaic/thermal solar systems. Sol Energy 2002;72(3):217–34.

[7] Ibrahim A, Othman MY, Ruslan MH, Mat S, Sopian K. Recent advances in flat plate photovoltaic/thermal (PV/T) solar collectors. Renew Sustain Energy Rev 2011;15:352–65. http://dx.doi.org/10.1016/j.rser.2010.09.024.

[8] Joe J, Iniyan S, Goic R. Flat plate solar photovoltaic – thermal (PV / T) systems: a reference guide. Renew Sustain Energy Rev 2015;51:62–88. http://dx.doi.org/10.1016/j.rser.2015.06.022.

[9] Renno C, Petito F. Design and modeling of a concentrating PV/T (CPV/T) system for a domestic application. Energy Build 2013;62:392–402.

[10] Vivar M, Everett V, Fuentes M, Blakers A, Tanner A, Le Lievre P, et al. Initial field performance of a hybrid CPV-T microconcentrator system. Prog Photovolt Res Appl 2013;21(8):1659–71.

[11] Brogren M, Nostell P, Karlsson B. Optical efficiency of a PV-thermal hybrid CPC module. In: Eurosun 2000-ISES Europe Solar Conference, Copenhagen. 625.
[12] Kong Chengdong, Zilin Xu, Yao Qiang. Outdoor performance of a low-concentrated photovoltaic–thermal hybrid system with crystalline silicon solar cells. Appl Energy 2013;112:618–25.
[13] Li Guiqiang, Pei Gang, Yang Ming, Ji Jie, Yuehong Su. Optical evaluation of a novel static incorporated compound parabolic concentrator with photovoltaic/thermal system and preliminary experiment. Energy Convers Manage 2014;85:204–11.
[14] Guiqiang Li, Gang Pei, Yuehong Su, Yunyun Wang, Jie Ji. Design and investigation of a novel lens-walled compound parabolic concentrator with air gap. Appl Energy 2014;125:21–7.
[15] Li Guiqiang, Pei Gang, Ji Jie, Yang Ming, Yuehong Su, Ning Xu. Numerical and experimental study on a PV/T system with static miniature solar concentrator. Sol Energy 2015;120:565–74.
[16] Li Guiqiang, Pei Gang, Ji Jie, Yuehong Su. Outdoor overall performance of a novel air-gap-lens-walled compound parabolic concentrator (ALCPC) incorporated with photovoltaic/thermal system. Appl Energy 2015;144:214–23.
[17] LESO-PB/EPFL, Enecolo AG, Ernst Schweizer AG, 2000. New generation of Hybrid Solar PV/T collectors, Swiss Federal Office of Energy. p. 1–55.
[18] Skoplaki E, Palyvos Ja. On the temperature dependence of photovoltaic module electrical performance: a review of efficiency/power correlations. Sol Energy 2009;83:614–24. http://dx.doi.org/10.1016/j.solener.2008.10.008.
[19] Abdelhamid M, Singh R, Qattawi A, Omar M, Haque I. Evaluation of on-board photovoltaic modules options for electric vehicles. IEEE J Photovolt 2014;4:1576–84. http://dx.doi.org/10.1109/JPHOTOV.2014.2347799.
[20] Abdelhamid M, Qattawi A, Singh R, Haque I. Comparison of an analytical hierarchy process and fuzzy axiomatic design for selecting appropriate photovoltaic modules for onboard vehicle design. Int J Mod Eng 2014;15:23–35.
[21] Coventry Joe S. Performance of a concentrating photovoltaic/thermal solar collector. Sol Energy 2005;78:211–22.
[22] Charalambous PG, Maidment GG, Kalogirou Sa, Yiakoumetti K. Photovoltaic thermal (PV/T) collectors: a review. Appl Therm Eng 2007;27:275–86. http://dx.doi.org/10.1016/j.applthermaleng.2006.06.007.
[23] Chow TT. A review on photovoltaic/thermal hybrid solar technology. Appl Energy 2010;87:365–79. http://dx.doi.org/10.1016/j.apenergy.2009.06.037.
[24] Hasan MA, Sumathy K. Photovoltaic thermal module concepts and their performance analysis: a review. Renew Sustain Energy Rev 2010;14:1845–59. http://dx.doi.org/10.1016/j.rser.2010.03.011.
[25] Zhang L, Jing D, Zhao L, Wei J, Guo L. Concentrating PV/T hybrid system for simultaneous electricity and usable heat generation: a review. Int J Photoenergy 2012;2012. http://dx.doi.org/10.1155/2012/869753.
[26] Tian Y, Zhao CY. A review of solar collectors and thermal energy storage in solar thermal applications. Appl Energy 2013;104:538–53. http://dx.doi.org/10.1016/j.apenergy.2012.11.051.
[27] Kumar A, Baredar P, Qureshi U. Historical and recent development of photovoltaic thermal (PVT) technologies. Renew Sustain Energy Rev 2015;42:1428–36. http://dx.doi.org/10.1016/j.rser.2014.11.044.
[28] Colangelo G, Favale E, Miglietta P, de Risi A. Innovation in flat solar thermal collectors: a review of the last ten years experimental results. Renew Sustain Energy Rev 2016;57:1141–59.
[29] Li M, Ji X, Li GL, Wei SX, Li YF, Shi F. Performance study of solar cell arrays based on a trough concentrating photovoltaic/thermal system. Appl Energy 2011;88(9):3218–27.
[30] Harper Da, Hildebrand RH, Stiening R, Winston R. Heat trap: an optimized far infrared field optics system. Appl Opt 1976;15:53–60. http://dx.doi.org/10.1364/AO.15.000053.
[31] Reflec Tech I. ReflecTech Mirror Film Technical DataAvailable from: http://www.reflectechsolar.com/pdfs/TechnicalData(ReflecTech).pdf2012 [accessed August 26, 2015].
[32] Winston R. Solar collectors with evacuated receiver and nonimaging external reflectors. US20040261788 A1; 2004.
[33] Burkholder F, Kutscher CF. Heat loss testing of Schott's 2008 PTR70 parabolic trough receiver; 2009.
[34] Silverman TJ, Deceglie MG, Marion B, Cowley S, Kayes B, Kurtz S. Outdoor performance of a thin-film gallium-arsenide photovoltaic module. Conf Rec IEEE Photovolt Spec Conf 2013:103–8. http://dx.doi.org/10.1109/PVSC.2013.6744109.
[35] MIRO-SUN® Test Report - alanod-solar.de; 2010: 1–20. <http://www.bluetec.eu/sites/default/files/pictures/MIRO_SUN_engl_101112_1.pdf> [accessed August 25, 2015].
[36] Coated Steel Tube, Himin Solar Co. Ltd. n.d. <http://www.himinsun.com/6-coated-steel.html> [accessed August 26, 2015].
[37] Omega, <http://www.omega.com/pptst/TJ36-ICIN.html>.
[38] Ashcroft, <bhttp://www.ashcroft.com/>.
[39] Yokogawa Corporation of America, <http://www.yokogawa.com/us/products/field-instruments/flow-meters/coriolis-flow-meter.htm#details:features>.
[40] The Eppley Laboratory, INC. <http://www.eppleylab.com/instrumentation/>.
[41] NREL. National Solar Radiation Data Base: 1991- 2005 Update: Typical Meteorological Year 3 n.d. <http://rredc.nrel.gov/solar/old_data/nsrdb/1991-2005/tmy3/> [accessed April 01, 2016].
[42] U.S Parabolic trough power plant data, National Renewable Energy Lab (NREL), <http://www.nrel.gov/csp/troughnet/power_plant_data.html> [accessed April 01, 2016].
[43] Turchi C. Parabolic trough reference plant for cost modeling with the Solar Advisor Model (SAM). National Renewable Energy Laboratory; 2010. p. 112. NREL/TP-550-47605.
[44] Kurup Parthiv, Turchi Craig S. Parabolic trough collector cost update for the System Advisor Model (SAM). National Renewable Energy Laboratory; 2015. Technical Report NREL/TP-6A20-65228 November 2015.
[45] Michael Woodhouse Alan Goodrich, A Manufacturing cost analysis relevant to single- and dual-junction photovoltaic cells fabricated with III-Vs and III-Vs Grown on Czochralski Silicon, NREL, NREL/PR-6A20-60126.
[46] Winston R, Eli Yablonovitch E, Jiang L, Widyolar BK, Abdelhamid M, et al. Hybrid solar collector using nonimaging optics and photovoltaic components. In: Proc SPIE 9572, nonimaging optics: efficient design for illumination and solar concentration XII, 957208 (August 25, 2015). http://dx.doi.org/10.1117/12.2191943.
[47] Cygan D, Abbasi H, Kozlov A, Pondo J, Winston R, Widyolar B, Jiang L, Abdelhamid M, Kirk AP, Drees M, Miyamoto H, Elarde VC, Osowski ML. Full Spectrum Solar System: Hybrid Concentrated Photovoltaic/Concentrated Solar Power (CPV-CSP). J Mater Res Soc Adv 2016. http://dx.doi.org/10.1557/adv.2016.512. Available on CJO.